

EFFICIENT MOTION DEBLURRING FOR INFORMATION RECOGNITION ON MOBILE DEVICES

Florian Brusius, Ulrich Schwanecke and Peter Barth
Hochschule RheinMain, Unter den Eichen 5, 65195 Wiesbaden, Germany

Keywords: Image processing, Blind deconvolution, Image restoration, Deblurring, Motion blur estimation, Barcodes, Mobile devices, Radon transform.

Abstract: In this paper, a new method for the identification and removal of image artifacts caused by linear motion blur is presented. By transforming the image into the frequency domain and computing its logarithmic power spectrum, the algorithm identifies the parameters describing the camera motion that caused the blur. The spectrum is analysed using an adjusted version of the Radon transform and a straightforward method for detecting local minima. Out of the computed parameters, a blur kernel is formed, which is used to deconvolute the image. As a result, the algorithm is able to make previously unrecognisable features clearly legible again. The method is designed to work in resource-constrained environments, such as on mobile devices, where it can serve as a preprocessing stage for information recognition software that uses the camera as an additional input device.

1 INTRODUCTION

Mobile devices have become a personal companion in many people's daily lives. Often, mobile applications rely on the knowledge of a specific context, such as location or task, which is cumbersome to provide via conventional input methods. Increasingly, cameras are used as alternative input devices providing context information – most often in the form of barcodes. A single picture can carry a large amount of information while at the same time, capturing it with the integrated camera of a smartphone is quick and easy. The processing power of smartphones has significantly increased over the last years, thus allowing mobile devices to recognise all kinds of visually perceptible information, like machine-readable barcode tags and theoretically even printed text, shapes, and faces. This makes the camera act as an one-click link between the real world and the digital world inside the device (Liu et al., 2008). However, to reap the benefits of this method the image has to be correctly recognised under various circumstances. This depends on the quality of the captured image and is therefore highly susceptible to all kinds of distortions and noise. The photographic image might be over- or underexposed, out of focus, perspective distorted, noisy or blurred by relative motion between the camera and the imaged object. Unfortunately, all of those

problems tend to occur even more on very small cameras. First, cameras on smartphones have very small image sensors and lenses that are bound to produce lower quality images. Second, and more important, the typical single-handed usage and the light weight of the devices make motion blur a common problem of pictures taken with a smartphone. In many cases, the small tremor caused by the user pushing the trigger is already enough to blur the image beyond machine or human recognition.

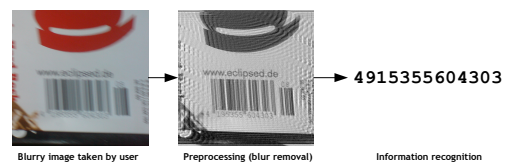


Figure 1: Use of the image deblurring algorithm as a preprocessing stage for information recognition software.

In order to make the information that is buried in blurry images available, the artefacts caused by the blur have to be removed before the attempt to extract the information. Such a preprocessing method should run in an acceptable time span directly on the device. In this paper, we present a method that identifies and subsequently removes linear, homogeneous motion blur and thus may serve as a preprocessing stage for information recognition systems (see figure 1).

2 RELATED WORK

In the last thirty-five years, many attempts have been made to identify and remove artefacts caused by image blur. Undoing the effects of linear motion blur involves three basic steps that can be considered as more or less separate from each other: Calculating the blur direction, calculating the blur extent, and finally using these two parameters to deconvolute the image. Since the quality of the deconvolution is highly dependent on the exact knowledge of the blur kernel, most publications focus on presenting new ways for blur parameter estimation. While some of the algorithms are developed to work upon a series of different images taken of the same scene (Chen et al., 2007; Sorel and Flusser, 2005; Harikumar and Bresler, 1999), the method in this paper attempts to do the same with a single image.

2.1 Blur Angle Calculation

Existing research can be divided into two groups: One that strives to estimate the blur parameters in the spatial image domain and another that tries to do the same in the frequency domain.

The former is based on the concept of motion causing uniform smear tracks of the imaged objects. (Yitzhaky and Kopeika, 1996) show that this smearing is equivalent to the reduction of high-frequency components along the direction of motion, while it preserves the high frequencies in other directions. Thus, one can estimate the blur angle by differentiating the image in all directions and determining the direction where the total intensity of the image derivative is lowest. However, this approach works best when the imaged objects are distinct from the background, so that the smears will look like distinct tracks. It also assumes that the original image has similar local characteristics in all directions. Such methods suffer from relatively large estimation errors (Wang et al., 2009). They also need a lot of computation time and therefore are not applicable to real time systems.

A more common approach is the blur direction

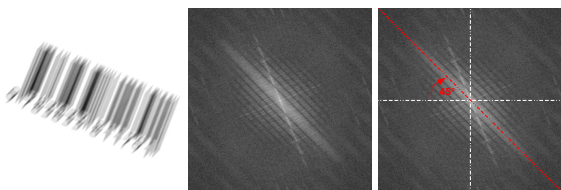


Figure 2: Image of a barcode blurred by linear camera motion in an angle of 45° and the resulting features in its logarithmic power spectrum.

identification in the frequency domain. (Cannon, 1976) showed that an image blurred by uniform linear camera motion features periodic stripes in the frequency domain. These stripes are perpendicular to the direction of motion (see figure 2). Thus, knowing the orientation of the stripes means knowing the orientation of the blur. In (Krahmer et al., 2006), an elaborate overview of the diverse methods for estimating linear motion blur in the frequency domain is presented. One possibility to detect the motion angle is the use of steerable filters, which are applied to the logarithmic power spectrum of the blurred image. These filters can be given an arbitrary orientation and therefore they can be used to detect edges of a certain direction. Since the ripples in the image's power spectrum are perpendicular to the direction of motion blur, the motion angle can be obtained by seeking the angle with the highest filter response value (Rekleitis, 1995). Unfortunately, this method delivers very inaccurate results. Another method of computing the motion direction analyses the cepstrum of the blurred image (Savakis and Easton Jr., 1994; Chu et al., 2007; Wu et al., 2007). This is based on the observation that the cepstrum of the motion blur point spread function (PSF) has large negative spikes at a certain distance from the origin, which are preserved in the cepstrum of the blurred image. In theory, this knowledge can be used to obtain an approximation of the motion angle by drawing a straight line from the origin to the first negative peak and computing the inverse tangent of its slope. However, this method has two major disadvantages. First, it only delivers good results in the absence of noise, because image noise will suppress the negative spikes caused by the blur. And second, calculating the cepstrum requires an additional inverse Fourier transform, which is computationally expensive. A third approach is the use of feature extraction techniques, such as the Hough or Radon transform. These operations detect line-shaped structures and allow for the determination of their orientations (Toft, 1996). The Hough transform, as it is used in (Lokhande et al., 2006), requires a preliminary binarisation of the log spectrum. Since the highest intensities concentrate around the center of the spectrum and decrease towards its borders, the binarisation threshold has to be calculated separately for each pixel, which can become computationally prohibitive. Another issue is that the stripes tend to melt into each other at the origin and thus become indistinct, which makes finding an adaptive thresholding algorithm that is appropriate for every possible ripple form a difficult, if not impossible task (Wang et al., 2009). The Radon transform is able to perform directly upon the unbinarised spectrum and is therefore

much more practical for time-critical applications. As a result, it delivers a two-dimensional array in which the coordinate of the maximum value provides an estimate of the blur angle. According to (Krahmer et al., 2006), the Radon transform delivers the most stable results. However, this method needs a huge amount of storage space and computation time.

2.2 Blur Length Calculation

The estimation of the blur extent in the spatial image domain is based on the observation that the derivative of a blurred image along the smear track emphasises the edges of the track which makes it possible to identify its length (Yitzhaky and Kopeika, 1996). Again, this method highly depends on distinctively visible smear tracks and is therefore very unstable. Most of the algorithms estimate the blur length in the frequency domain, where it corresponds to the breadth and frequency of the ripples. The breadth of the central stripe and the gaps between the ripples are inversely proportional to the blur length. To analyse the ripple pattern, usually the cepstrum is calculated. One way of computing the blur extent is to estimate the distance from the origin where the two negative peaks become visible in the cepstrum. After rotating the cepstrum by the blur angle, these peaks appear at opposite positions from the origin and their distance to the y-axis can easily be determined (Chu et al., 2007; Wu et al., 2007). Another way collapses the logarithmic power spectrum onto a line that passes through the origin at the estimated blur angle. This yields a one-dimensional version of the spectrum in which the pattern of the ripples becomes clearly visible, provided that the blur direction has been calculated exactly enough. By taking the inverse Fourier transform of this 1-D spectrum, which can be called the 1-D cepstrum, and therein seeking the coordinate of the first negative peak, the blur length can be estimated (Lokhande et al., 2006; Rekleitis, 1995). As with the angle estimation, these two methods have their specific disadvantages: In the first method, calculating the two-dimensional cepstrum is a comparatively expensive operation, while the second method is once again highly susceptible to noise.

2.3 Image Deblurring

Knowing the blur parameters, an appropriate PSF can be calculated. This blur kernel then can be used to reconstruct an approximation of the original scene out of the distorted image (Krahmer et al., 2006). Unfortunately, traditional methods like Wiener or Lucy-Richardson filter tend to produce additional artefacts

of their own in the deconvoluted images (Chalkov et al., 2008). These artefacts particularly occur at strong edges and along the borders of the image. Some methods have been developed to overcome that issue, such as in (Shan et al., 2008), where a new model for image noise is presented. However, these methods always involve some sort of iterative optimisation process, which is repeated until the result converges towards an ideal. This makes them inappropriate for the use in time-critical applications. Luckily, there is no need to get rid of all the artefacts, as long as the information contained in the image is recognisable. However, it has to be taken into account that the deconvolution artefacts may still hinder or complicate the recognition process.

3 THE IMAGE DEGRADATION MODEL

In order to support the elimination or reduction of motion blur, a mathematical model that describes this degradation is needed. When a camera moves over a certain distance during exposure time, every point of the pictured scene is mapped onto several pixels of the resulting image and produces a photography that is blurred along the direction of motion. This procedure can be regarded as some sort of distortion of the unblurred original image, i.e. the picture taken without any relative movement between the camera and the imaged scene. The distortion can be modelled as a linear filter function $h(u, v)$ that describes how a point-shaped light source would be mapped by the photography and which is therefore called the point spread function (PSF). Thus, the blurring of an original image $f(u, v)$ (see figure 3) equates to the linear convolution $*$ with the adequate PSF (Cannon, 1976). In the case of linear homogeneous motion blur, this PSF is a one-dimensional rectangular function (Lokhande et al., 2006). The PSF looks like a line through the point of origin with the angle φ to the x-axis, equal to the direction of motion, and the length L , equal to the distance one pixel travels along this direction of motion. The coefficients in $h(u, v)$ sum up to 1, thus the intensity being $1/L$ along the line and 0 elsewhere. With the knowledge of the correct motion parameters, the PSF can be calculated via

$$h(u, v) = \begin{cases} \frac{1}{L} & \text{if } (u, v) \begin{pmatrix} \sin \varphi \\ \cos \varphi \end{pmatrix} = 0 \text{ and } u^2 + v^2 < (\frac{L}{2})^2 \\ 0 & \text{otherwise} \end{cases} \quad (1)$$

It has to be taken into account that in the majority of cases, the undistorted original image is deranged by additional, signal-independent noise. This noise can be modelled as an unknown random function $n(u, v)$, which is added to the image. Hence, the blurred image $i(u, v)$ can be described as

$$i(u, v) = f(u, v) * h(u, v) + n(u, v) . \quad (2)$$

Because the convolution becomes a multiplication in the frequency domain, the Fourier transform of the blurred image equates to

$$I(m, n) = F(m, n) \cdot H(m, n) + N(m, n) . \quad (3)$$

This multiplication could theoretically be reversed by pixel-wise division, so with the knowledge of the proper PSF, the undistorted original image could be obtained through the inverse Fourier transform. This procedure is often referred to as *inverse filtering* (Gonzalez and Woods, 2008). However, this only works properly under the assumption that there is zero noise. In the presence of noise, only an approximation \hat{F} of the transformed original image can be obtained, which equals to

$$\begin{aligned} \hat{F} &= \frac{I(m, n)}{H(m, n)} = \frac{F(m, n) \cdot H(m, n) + N(m, n)}{H(m, n)} \\ &= F(m, n) + \frac{N(m, n)}{H(m, n)} . \end{aligned} \quad (4)$$

This shows that \hat{F} cannot be reconstructed without the knowledge of the transformed noise function N . In addition, the small coefficients in $H(m, n)$ make the term $N(m, n)/H(m, n)$ very large and superpose the actual original image beyond recognition (Gonzalez and Woods, 2008). To avoid that, a method of inverse filtering is needed that explicitly takes the noise signal into consideration. The Wiener deconvolution is such a method, which is based on the well known Wiener filter (Wiener, 1949) for noise suppression in signal processing.

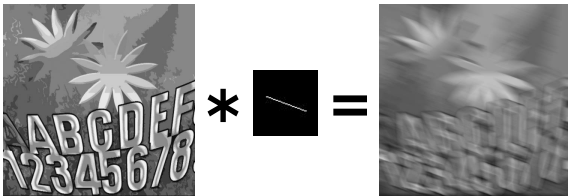


Figure 3: Motion blur can be modelled as a linear convolution with an appropriate PSF.

4 THE IMAGE DEBLURRING ALGORITHM

In the algorithm presented in this paper, a given blurred input image is analysed to determine the direction and length of the camera movement that caused the blur. These two motion parameters are used to calculate a point spread function modelling the blur. Regarding the blur as a linear convolution of the original image with that blur kernel, it can be removed by reversing this operation. The algorithm focuses on efficient computation and is therefore suitable for resource-limited environments.

First, in section 4.1 a *preprocessing* step, which converts a relevant part of the respective greyscale image to the frequency domain with FFT, is introduced. Then, in section 4.2 the *blur direction* is determined by performing a Radon transform on the logarithmic power spectrum of the blurred image. The power spectrum features some ripples in its centre, which run perpendicular to the direction of motion. The computation time of the Radon transform is significantly decreased by customising it to fit the structural conditions of the spectrum. Next, in section 4.3 the *blur length* is estimated by measuring the breadth of the central ripple within the log spectrum, which is inversely proportional to the sought-after blur length. This is done by collapsing the spectrum onto a line that passes through its origin at an estimated blur angle. Then the resulting one-dimensional log spectrum is analysed to find the first significant local minimum. This approach does not require any further costly Fourier transforms. In the last step in section 4.4, the PSF is calculated and a simple Wiener filter is used to *deconvolute* the image.

Figure 4 shows an overview of the algorithm. It also denotes the additional costly segmentation of the image that is required if instead of the Radon transform the Hough transform is used to detect the blur direction.

4.1 Preprocessing

Estimating the blur parameters requires some preprocessing. First, the colour image obtained by the smartphone camera is converted into an 8 bit-greyscale picture. This can be done by averaging the colour channels or by weighting the RGB-parts according to the luminance perception of the human eye (Burger and Burge, 2008).

$$i'(u, v) = 0.30 \cdot i_R(u, v) + 0.59 \cdot i_G(u, v) + 0.11 \cdot i_B(u, v) \quad (5)$$

Next, a square section is cut out of the centre of the image. For the FFT to be applicable, this size has to

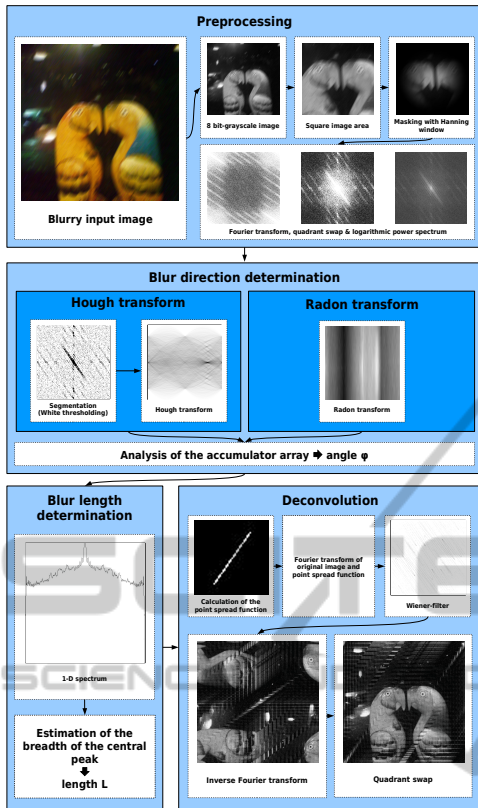


Figure 4: Overview of the image deblurring algorithm.

be a power of two. In practise, sizes of 512×512 and 256×256 pixels have shown to maintain a reasonable balance between stable high quality results and computational cost. The period transitions from one image border to the next often lead to high frequencies, which become visible in the image's power spectrum as vertical and horizontal lines. Since these lines may distract from or even superpose the stripes caused by the blur, they have to be eliminated by applying a windowing function before transforming the image. The Hanning window offers a good trade-off between forming a smooth transition towards the image borders and preserving a sufficient amount of image information for the parameter estimation. For a square image of size M , the Hanning window is calculated as (Burger and Burge, 2008)

$$w_{\text{Hanning}}(u, v) = \begin{cases} 0.5 \cdot \cos(\pi r_{u,v} + 1) & \text{if } 0 \leq r_{u,v} \leq 1 \\ 0 & \text{otherwise} \end{cases}$$

with

$$r_{u,v} = \sqrt{\left(\frac{2u}{M} - 1\right)^2 + \left(\frac{2v}{M} - 1\right)^2}. \quad (6)$$

After that step, the windowed image can be transferred into the frequency domain by performing a FFT. To facilitate the identification of particular features of the Fourier spectrum, its power spectrum is computed. In its basic form, the power spectrum is defined as the absolute value of the Fourier transformed image. However, because the coefficients of the Fourier spectrum decrease rapidly from its center towards the borders, it can be difficult to identify local differences. Taking the logarithm of the power spectrum $s(u, v) = \log |I(m, n)|$ helps to balance this rapid decrease. In order to obtain a centred version of the spectrum, its quadrants have to be swapped diagonally. Since the interesting features are around the centre of the spectrum, the following operations can be performed upon a centred 256×256 -window, which reduces computation time.

4.2 Blur Direction Determination

As a result of the above operations, the power spectrum exhibits a pattern of stripes parallel to a line passing through its origin at an angle θ , which corresponds to the motion angle ϕ as $\theta = -\phi$. Thus, estimating the direction of these stripes means knowing the motion angle. To do so, a Radon transform is performed. This is done by shooting a certain amount of parallel rays for each possible angle θ through the image, adding up the intensities of the pixels hit by each ray and subsequently storing the sums in a two-dimensional accumulator array. The high intensity values along the sought-after stripes lead to local maxima within this array, and the corresponding array indices reveal the parameters (radius and angle) of the detected lines. The precision of the algorithm depends on how fine the angle domain $\theta = 0 \dots \pi$ is divided into a number of n_θ steps. 360 steps provide an accuracy of 0.5° , which is sufficient for image reconstruction and subsequent information extraction.

In the general case where the position of the sought-after feature is unknown, there is no alternative but to try every possible distance for each angle (see figure 6(a)). Yet with the previous knowledge that the central stripe runs through the origin, the radius is always 0 and the complexity of the procedure can be significantly decreased. Theoretically, all what has to be done is to shoot one ray per angle through the origin of the spectrum and determine the angle with the highest sum (see figure 6(b)).

Unfortunately, this method usually fails in practise. Periodic structures are common in e.g. barcodes and high-contrast edges occur for example along the border of a white sheet of paper photographed against a dark background. In the spectrum they manifest as

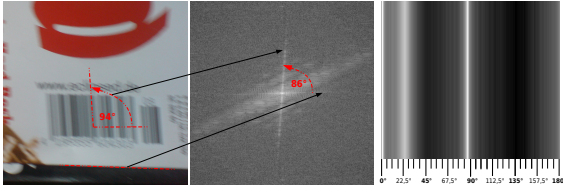


Figure 5: The periodic structures of the barcode lead to additional features in the power spectrum and create distracting maxima in the Radon accumulator array.

additional lines (see figure 5). Since these distracting parts tend to have very high frequencies, they can easily lead to wrong estimations. Therefore, a criterion is needed which helps to separate the “wrong” features from the “right” ones. Fortunately, the breadth of the central stripe caused by the blur is inversely proportional to the blur length. This means that for typical cases of motion blur up to 50-70 pixels, the blur stripe is much broader than the distracting other stripes. At the same time, it is also more diffuse, meaning that it spreads its energy over its breadth. The correct angle can reliably be estimated by looking for maxima within the expected breadth from the origin only (see figure 6(c)). This is a nontrivial problem, because the blur length and with it the expected breadth b are not known. Since taking a value for b that is significantly larger than the actual breadth would lead to an inaccurate estimation, the best result can be achieved by choosing b according to the largest expected blur length (which corresponds to the smallest expected ripple breadth). The blur length is equal to the size of the spectrum divided by the half of b . Hence, for a length of 60 pixels, b equates to $\frac{1}{30}$ of the spectrum width.

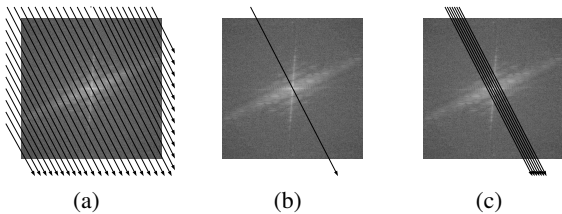


Figure 6: Three different versions of the Radon transform. The arrows denote the rays shot through the image for one particular angle. In (a), every single possible radius is taken into account, whereas (b) and (c) are individually customised to the expected structure of the power spectra.

The result is an array with $n_\theta \cdot b$ sums. Determining the correct blur angle out of this array is done by searching for the w consecutive angles whose sums add up to the highest total sum. Each of these sums consists of b single values, according to the number of rays sent through the image for each angle. Having

found these w angles, the maximum out of all $w \cdot b$ single values is determined. The angle to whose sum this maximum value has contributed is the desired angle of camera motion. A range of 3° has proven to be sufficiently large to ensure that the correct angle is selected, so that w can be calculated out of the angle resolution n_θ .

$$w = \frac{n_\theta}{180} \cdot 3 \quad (7)$$

4.3 Blur Length Determination

The blur length is also calculated by analysing the logarithmic power spectrum of the blurred image. Here, it is the breadth of the central ripple running through the origin that has to be estimated. This breadth is inversely proportional to the blur extent and therefore can be used to calculate it. Unlike the majority of other algorithms, the estimation requires no further Fourier transform. To determine the breadth of the central stripe, a one-dimensional version of the spectrum is calculated. This is done by collapsing the intensity values of the spectrum onto a line running through the origin perpendicular to the blur ripples. The intensity of each pixel is summed up in an array according to its distance d from that line. In order to do so, d has to be discretised first. Since simple rounding may lead to imprecise results, (Rekleitis, 1995) proposes another approach where the intensities are proportionately divided into two array indexes according to the decimal places of their distances from the projection line. He also suggests to normalise the projected spectrum by dividing each sum by the amount of pixels that went into it. That way, the sums do not necessarily decrease towards the borders of the array, because fewer pixels contribute to them. In addition to these two improvements, (Krahmer et al., 2006) proposes to mirror the array in its centre and to add the values to the respective other side. Due to the fact that the blur ripples should be symmetric, this suppresses noise and at the same time clarifies the interesting features.

The resulting 1-D spectrum exhibits a prominent peak in its centre which matches the central blur ripple in the 2-D spectrum (see figure 7). The zeros, or rather the gaps, between the individual stripes manifest as local minima in the collapsed spectrum. To identify the maximum in the centre of the spectrum, a search to the right (either direction would be possible because of the symmetry) is performed until the values become higher instead of smaller.

$$P(x_0) < P(x_0 + 1) \quad (8)$$

Out of this first local minimum x_0 , one easily can calculate the breadth of the blur ripple by doubling its

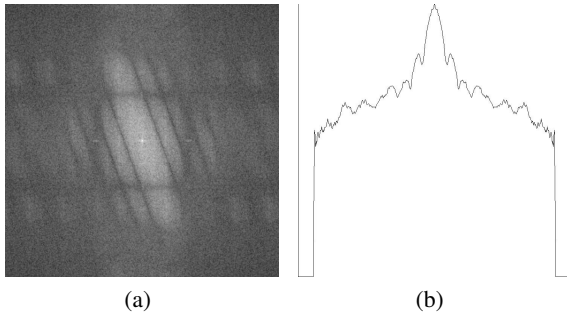


Figure 7: The log power spectrum of a blurred image (a) and the plot of its projected 1-D spectrum (b).

distance to the maximum. Unfortunately, this simple approach usually fails in the presence of noise. With blur that has been developed under realistic conditions, small deflections show up in the spectrum. Thus, the collapsed spectrum is not monotonically decreasing up to the sought-after first local minimum and the approach described in (8) is bound to fail. To solve this problem, we propose to define a distance s within which the values must not become bigger than at the potential minimum.

$$P(x_0) < P(x_0 + 1) < P(x_0 + s) \quad (9)$$

Since the parallel ripples in the spectrum become smaller and more dense to the same degree the causing movement is faster, the choice of a proper value for s is not an easy one. On the one hand, it has to be larger than the maximal breadth of the noise deflections it strives to suppress. On the other hand, it has to be smaller than the minimal breadth of the next ripple, which is half as broad as the one in the centre. This means that s has to be individually computed according to the characteristics of the present spectrum. With increasingly larger blur lengths, the values in the spectrum decline more rapidly towards the sides. This is why the calculation of the slope m between two points $Q_1 = (x_1, y_1)$ and $Q_2 = (x_2, y_2)$, which both lie on the central peak, is a promising approach. To be on the safe side, we presume a maximal blur length of 100 pixels, which would make the breadth of the entire peak $\frac{1}{50}$ of the width $\sqrt{2}M$ of the spectrum. Hence, x_1 is set to be at the centre $M/\sqrt{2}$ and x_2 at a distance of $\frac{1}{100}$ of the spectrum width from there.

$$m = \left| \frac{y_2 - y_1}{x_2 - x_1} \right| = \left| \frac{P(x_2) - P(x_1)}{\frac{1}{100} \sqrt{2}M} \right| \quad (10)$$

The resulting slope m grows with increasingly larger blur lengths. At the same time, the deflections become smaller as the slope becomes steeper, which means that smaller blur lengths are more susceptible

to noise than larger ones. Thus, for determining s , we use the reciprocal of m , multiplied by an appropriate correction factor f :

$$s = \frac{1}{m} \cdot f \quad (11)$$

For a spectrum with a size of 512×512 pixels, we found that dividing the slope by a correction factor of 5 worked best. Since the breadths of the peaks depend on the size M of the projected power spectrum, this results in a correction factor of $f = \frac{M}{2560}$:

$$s = \frac{1}{m} \cdot f = \frac{1}{m} \cdot \frac{M}{512 \cdot 5} = \frac{M}{2560 \cdot m} \quad (12)$$

When the correct minimum x_0 has been found according to equation (9), the breadth b of the peak is calculated as

$$b = 2 \cdot \left(x_0 - \frac{M}{\sqrt{2}} \right) \quad (13)$$

Because b is inversely proportional to the length L of the camera motion, the reciprocal of b is used. L is then calculated by dividing the size of the spectrum by the half of b .

$$L = \frac{2M}{b} \quad (14)$$

It is possible that the algorithm fails to detect a local minimum. This is mostly due to a faulty calculation of the distance s or the collapsed spectrum exhibiting no prominent peaks. The latter is the case when the angle has not been estimated exactly enough in the previous step, which leads to an incorrect projection line orientation.

4.4 Deconvolution

Knowing the two blur parameters, an adequate PSF can be calculated according to equation (1). Then both the PSF and the original, unaltered image have to be transformed into the frequency domain so that the deconvolution can be carried out. The Wiener deconvolution filter as it is presented in (Lokhande et al., 2006) is given by

$$\hat{F} = \frac{H^*(m, n) \cdot I(m, n)}{H^*(m, n) \cdot H(m, n) + K} \quad (15)$$

where $H^*(m, n)$ is the complex conjugate of $H(m, n)$ and K is a constant that can be approximated by the reciprocal image width $1/B$. In order to obtain the reconstructed, deblurred image, the result eventually has to be transformed back into the image domain.

Provided that the information in the pictured object consists solely of monochrome elements, it might be reasonable to binarise the reconstructed image. Good results can be achieved with the thresholding

algorithms of White (White and Rohrer, 1983) and Bernsen (Sezgin and Sankur, 2004). Since most of the locally-adaptive thresholding methods require a lot of computation time, this method is better used in environments that are not time critical. However, if the photo is consistently lit so that a viable global threshold can be found, the method of Otsu (Otsu, 1979) might also be applicable.

5 EVALUATION

In order to evaluate how accurate and reliable the motion parameter estimation works, two different classes of input data have been used. The first category consisted of images with artificially generated motion blur. To do so, 11 different motifs had each been convoluted with 30 different PSFs. These PSFs had been constructed from all possible combinations out of five different, randomly chosen angles and six different, likewise random lengths according to the definition given by equation (1). This way, a total of 330 test images were created. The original motifs comprised real photography as well as completely digitally created pictures, all of a size of 512×512 pixels.

Nine of the images showed different kinds of barcodes. The benefit of artificially created blur is that the exact motion parameters are known beforehand and can therefore easily be compared to the ones determined by the algorithm. Yet it can not predict whether the method works for photos taken under real conditions. Hence, the second class consisted of real, unaltered photographs. For these pictures, five different barcodes had each been photographed five times. In order to simulate realistic conditions, they were made using a smartphone camera, manually moving the phone in different speeds and angles during exposure time. The shots were also taken under different light conditions in order to vary the shutter speed.

5.1 Artificial Blur

For the artificially blurred images, the angle estimation continuously produced stable results. The algorithm could estimate the angles up to an accuracy of 5° for 92.71% of the test images. In most of the cases where the estimation delivered incorrect results, this was caused by additional features in the power spectrum induced by periodic structures or high-contrast edges. The accuracy of the angle estimation is to some degree dependent on the intensity of the blur: If the ray within which the Radon transform sums up the intensity values is smaller than the stripe it strives to detect, multiple maxima occur at adjacent angles.

Since shorter blur lengths lead to broader stripes, the accuracy decreases with the blur length, as can be seen in table 1. Only taking into account pictures with blur lengths greater than 50 pixels leads to an increase of the detection rates for 0.5° accuracy of 40% of the images. Out of the pictures with blur lengths greater than 30 pixels, nearly 100% could be detected correctly with an accuracy of 4° .

The blur length estimation also worked reliably, provided that the angle had been calculated correctly. In the case of an exact angle estimation in the range of 0.5° around the desired value, 95.73% of the blur lengths could be determined with an accuracy up to 5 pixels. As shown in table 2, this rate decreases to 79.43% for an angle estimation accuracy of 5° . Given these numbers, the percentage of images where both the angle and the length could be estimated with an accuracy of up to 5° or 5 pixels, is 73.56%. Nevertheless, the high portion of correctly estimated blur lengths with the exact knowledge of the blur angle shows that the method for blur length estimation presented in this paper works well. The accuracy however decreases for greater blur lengths, which is once again due to the breadth of the central ripple: In a spectrum of the size of 256 pixels, it is 26 pixels broad for a blur length of 20 pixels. If the blur length is doubled to 40 pixels, the breadth is halved accordingly to 13 pixels. For a blur length of 80 pixels, the stripe is merely 6 pixels broad. The breadth of the ripple converges towards the resolution limit and the accuracy with which it can be determined inevitably decreases.

5.2 Real Blur

To allow the verification of the blur parameters estimated for photos taken under real conditions, the angles of the ripples appearing in the images' power spectra were measured manually. The same was done for the blur lengths using plots of the 1-D spectra. Since the estimation of the blur length is impossible without the exact knowledge of the corresponding blur angle, in cases where the angle estimation had failed the spectra were recreated using the manually measured data. In other words, corrective actions were taken in order to make separate statements about the estimation accuracy of both parameters.

The test material presented here can only attempt to provide evidence of the algorithm's performance under real conditions. On the one hand, the amount of images is much smaller than that with the artificially created blur. On the other hand, even the images taken with a smartphone camera were likewise created "artificially", since they all had been taken with the explicit intent to create linear motion blur. Yet, it can

Table 1: Angle detection rates for angles with artificial blur.

accuracy up to	maximal blur length					
	all	≥ 25 px	≥ 30 px	≥ 40 px	≥ 50 px	≥ 70 px
0.5°	35.56%	41.82%	45.00%	48.48%	50.00%	47.27%
1.5°	64.13%	74.55%	79.09%	84.24%	87.27%	89.09%
2°	76.60%	86.55%	90.91%	94.55%	94.55%	94.55%
3°	86.32%	96.36%	97.27%	98.18%	97.27%	96.36%
4°	89.06%	98.55%	99.55%	99.39%	99.09%	98.18%
5°	92.71%	99.27%	99.55%	99.39%	99.09%	98.18%
7°	95.44%	99.64%	99.55%	99.39%	99.09%	98.18%
10°	95.44%	99.64%	99.55%	99.39%	99.09%	98.18%
\varnothing deviation	3.01°	1.36°	1.28°	1.25°	1.36°	1.82°

Table 2: Length detection rates for artificial blur.

accuracy up to	maximal accuracy of the angle estimation						
	0.5°	1.5°	2°	4°	5°	10°	all
1 px	15.38%	17.54%	17.86%	18.77%	19.02%	19.43%	18.84%
2 px	49.57%	45.97%	46.03%	46.08%	47.21%	48.09%	46.20%
3 px	74.36%	66.35%	63.10%	61.43%	62.30%	62.74%	60.49%
4 px	95.73%	82.94%	78.57%	76.11%	76.39%	76.43%	73.56%
5 px	95.73%	84.83%	81.75%	79.18%	79.34%	79.62%	76.90%
7 px	99.15%	90.52%	86.51%	83.96%	83.93%	84.08%	81.76%
10 px	99.15%	92.89%	88.89%	87.71%	87.87%	87.90%	86.63%
\varnothing deviation	6.08 px	6.46 px	9.24 px	8.99 px	8.74 px	8.62 px	9.08 px

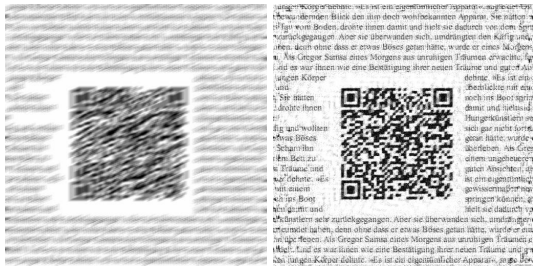
be stated that the method generally works for motion blur caused by actual movement of a physical camera. Table 3 shows that for 16 out of the 25 images, the motion angle could be estimated with a 5°-accuracy, which still is a detection rate of roughly 60%. The lengths could be estimated accurately to 5 pixels in 14 out of 25 cases. When the exact angles from the manual measuring were used, this rate increased to 22 out of 25 (88%).

5.3 Image Reconstruction

In the last step, the algorithm uses the determined motion parameters to remove the blur artefacts. The images in figure 8 clearly show that the reconstruction is able to produce good results: Text that could not even be identified as such becomes legible again, and individual elements of the barcodes become clearly disti-

nguishable. Figure 8(b) shows that even with very large blur lengths of around 70 pixels, still good results are possible. While the results are of course better with the artificial blur, the naturally blurred images also could be successfully deblurred in many cases.

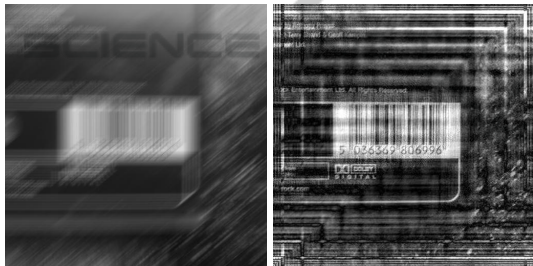
To determine whether the deblurring allows for increased detection rates of barcode scanners, some test images were passed through the open source ZXing-Decoder before and after the reconstruction. Out of the artificially blurred images, 50 were chosen where the barcode elements were distinctively visible. With these 50 images, the detection rates of the ZXing-Decoder could be increased by 30.6%. An additional binarisation of the resulting images using the method of Bernsen could increase the success rate by another 4.1%. There, among the images with less than 15 pixels blur length the increase was 41.7% in total. Extrapolated onto all images that could have been



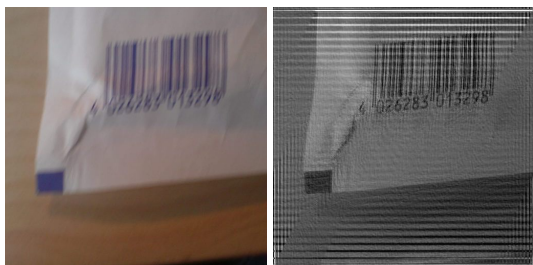
(a) Artificial blur. Angle: 22.5°, length: 25 pixels.



(b) Artificial blur. Angle: 74.5°, length: 70 pixels.



(c) Artificial blur. Angle: 40°, length: 50 pixels.



(d) Real blur. Angle: 63°, length: 16.52 pixels.



(e) Real blur. Angle: 156°, length: 11.38 pixels.

Figure 8: Images blurred by artificial ((a), (b), (c)) and real ((d), (e)) linear motion and their respective deconvolution results.

Table 3: Comparison between the manual measuring and the values determined by the algorithm for the 25 test images. Deviations of more than 5 pixels are highlighted.

	angle (manual)	angle (algorithm)	length (manual)	length (algorithm)
	100.0°	89.5°	14.22 px	14.63 px
	180.0°	178.0°	17.96 px	18.29 px
	38.0°	36.0°	34.13 px	36.57 px
	90.0°	89.0°	21.79 px	22.26 px
	32.0°	32.5°	26.95 px	28.44 px
	150.0°	98.0°	11.38 px	11.38 px
	90.0°	90.5°	25.6 px	25.6 px
	42.0°	86.0°	8.46 px	9.31 px
	1.0°	1.5°	20.9 px	85.33 px
	63.0°	86.5°	16.0 px	16.52 px
	91.0°	90.0°	9.23 px	46.55 px
	7.0°	0.5°	15.28 px	8.53 px
	156.0°	1.5°	11.38 px	11.38 px
	62.0°	93.0°	10.04 px	11.64 px
	59.0°	61.5°	14.42 px	14.22 px
	178.0°	1.5°	14.22 px	14.63 px
	91.0°	90.5°	15.75 px	15.06 px
	12.0°	3.5°	6.4 px	4.92 px
	140.0°	177.0°	14.03 px	4.92 px
	171.0°	173.0°	8.83 px	8.83 px
	179.0°	180.0°	9.23 px	20.48 px
	174.0°	177.5°	15.28 px	18.96 px
	75.0°	78.5°	8.53 px	2.67 px
	142.0°	146.0°	14.42 px	14.63 px
	45.0°	49.0°	14.63 px	15.52 px

recognised theoretically, this gives a rate of 8.1%. Note, that even then the percentage of images on which the reconstructed information is recognisable with the naked eye is much higher. Obviously, the scanning algorithm cannot handle the reconstructed input images. This is most likely due to the additional artefacts and diffuse edges caused by the deconvolution (Shan et al., 2008).

5.4 Performance

The algorithm has been implemented in Java in order to conduct the experiments. It was first run on a standard desktop PC (3 GHz Intel Pentium D with 2 GB

RAM) using JavaSE 1.6 and then ported to JavaME in order to test it on a real mobile device. In the test run, the whole process (preprocessing, blur parameter estimation and deconvolution) took about 500 ms for all images to be completed on the desktop computer. The exact same calculation took a total of about 22 seconds on a last generation mobile device (*Sony Ericsson k800i*), which is more than 40 times longer. While some parts (e.g. the windowing) ran about 23 times slower on the smartphone than on the desktop PC, the FFT took 90 times as long. For the FFT the comparatively much slower floating point arithmetic makes itself felt. However, note that next generation hardware offers higher integer performance, much better floating point support, and faster Java run time environments. An analysis on the desktop computer revealed that the FFT by far required the longest CPU time (36%), followed by the Radon transform (18%) and the calculation of the power spectrum (8%). Since the complexity of the FFT is $O(M \log M)$, dependent on the image size M , this also determines the complexity of the deblurring algorithm as a whole.

6 CONCLUSIONS AND FUTURE WORK

In this paper, a novel method combining and adapting existing techniques for the estimation of motion blur parameters and the subsequent removal of this blur is presented. The algorithm is suitable for the execution on resource-constrained devices such as modern smartphones and can be used as a preprocessing phase for mobile information recognition software.

The algorithm uses the logarithmic power spectrum of a blurred image to identify the motion parameters. It introduces a new, specially adjusted and therefore time-saving version of the Radon transform for angle detection where features are only sought after within a certain distance around the origin. The blur length is detected by analysing a one-dimensional version of the spectrum. No cepstrum and hence no further FFT are required. The estimated parameters are then used to form a proper PSF with which the blurred image can be deconvoluted. To do so, a Wiener filter is employed.

It was found that the motion angle estimation worked with a 5° accuracy for 92.71% of 330 artificially blurred images. The blur length determination delivered correct results with a maximum error of 5 pixels in 95.73% of all cases. For images blurred by real movement of an actual camera, these rates amounted to roughly 60% and 88%, respectively. The algorithm was implemented in Java to run on desk-

top computers as well as mobile devices. The algorithm terminated within 500 ms on a standard desktop computer and took around 40 times longer on an older smartphone. While sub second performance on smartphones is not to be expected any time soon, execution time within a few seconds on modern hardware should be attainable.

The application of the presented algorithm makes some previously unrecognised barcodes to be recognised by the ZXing decoder. However, the additional artefacts caused by the deconvolution itself often hinders the recognition in other cases. Yet, after the deconvolution, completely blurred text become legible again, and individual barcode features become clearly distinguishable in many of the cases where decoding failed. This gives reason to surmise that a successful recognition might be possible if the decoders were able to cope with the singularities of the reconstructed images. Or, deconvolution methods that suppress the emergence of artefacts could be explored.

REFERENCES

- Burger, W. and Burge, M. J. (2008). *Digital Image Processing – An Algorithmic Introduction Using Java*. Springer.
- Cannon, M. (1976). Blind deconvolution of spatially invariant image blurs with phase. *Acoustics, Speech and Signal Processing, IEEE Transactions on*, 24(1), pages 58–63.
- Chalkov, S., Meshalkina, N., and Kim, C.-S. (2008). Post-processing algorithm for reducing ringing artefacts in deblurred images. In *The 23rd International Technical Conference on Circuits/Systems, Computers and Communications (ITC-CSCC 2008)*, pages 1193–1196. School of Electrical Engineering, Korea University Seoul.
- Chen, L., Yap, K.-H., and He, Y. (2007). Efficient recursive multichannel blind image restoration. *EURASIP J. Appl. Signal Process.*, 2007(1).
- Chu, C.-H., Yang, D.-N., and Chen, M.-S. (2007). Image stabilization for 2d barcode in handheld devices. In *MULTIMEDIA '07: Proceedings of the 15th International Conference on Multimedia*, pages 697–706, New York, NY, USA. ACM.
- Gonzalez, R. C. and Woods, R. E. (2008). *Digital Image Processing*. Pearson Education Inc.
- Harikumar, G. and Bresler, Y. (1999). Perfect blind restoration of images blurred by multiple filters: Theory and efficient algorithms. *Image Processing, IEEE Transactions on*, 8(2), pages 202–219.
- Krahmer, F., Lin, Y., McAdoo, B., Ott, K., Wang, J., Widmann, D., and Wohlberg, B. (2006). Blind image deconvolution: Motion blur estimation. Technical report, University of Minnesota.

- Liu, Y., Yang, B., and Yang, J. (2008). Bar code recognition in complex scenes by camera phones. In *ICNC '08: Proceedings of the 2008 Fourth International Conference on Natural Computation*, pages 462–466, Washington, DC, USA. IEEE Computer Society.
- Lokhande, R., Arya, K. V., and Gupta, P. (2006). Identification of parameters and restoration of motion blurred images. In *SAC '06: Proceedings of the 2006 ACM Symposium on Applied Computing*, pages 301–305, New York, NY, USA. ACM.
- Otsu, N. (1979). A threshold selection method from gray-level histograms. *IEEE Transactions on Systems, Man and Cybernetics*, 9(1), pages 62–66.
- Rekleitis, I. (1995). Visual motion estimation based on motion blur interpretation. Master's thesis, School of Computer Science, McGill University, Montreal.
- Savakis, A. E. and Easton Jr., R. L. (1994). Blur identification based on higher order spectral nulls. *SPIE Image Reconstruction and Restoration* (2302).
- Sezgin, M. and Sankur, B. (2004). Survey over image thresholding techniques and quantitative performance evaluation. *Journal of Electronic Imaging*, 13(1), pages 146–168.
- Shan, Q., Jia, J., and Agarwala, A. (2008). High-quality motion deblurring from a single image. *ACM Trans. Graph.*, 27(3), pages 1–10.
- Sorel, M. and Flusser, J. (2005). Blind restoration of images blurred by complex camera motion and simultaneous recovery of 3d scene structure. In *Signal Processing and Information Technology, 2005. Proceedings of the Fifth IEEE International Symposium on*, pages 737–742.
- Toft, P. (1996). *The Radon Transform – Theory and Implementation*. PhD thesis, Electronics Institute, Technical University of Denmark.
- Wang, Y., Huang, X., and Jia, P. (2009). Direction parameter identification of motion-blurred image based on three second order frequency moments. *Measuring Technology and Mechatronics Automation, International Conference on* (1), pages 453–457.
- White, J. and Rohrer, G. (1983). Image thresholding for optical character recognition and other applications requiring character image extraction. *IBM J. Res. Dev.*, 27, pages 400–411.
- Wiener, N. (1949). *Extrapolation, Interpolation, and Smoothing of Stationary Time Series*. Wiley, New York.
- Wu, S., Lu, Z., Ping Ong, E., and Lin, W. (2007). Blind image blur identification in cepstrum domain. In *Computer Communications and Networks, 2007. ICCCN 2007. Proceedings of 16th International Conference on*, pages 1166–1171.
- Yitzhaky, Y. and Kopeika, N. (1996). Evaluation of the blur parameters from motion blurred images. In *Electrical and Electronics Engineers in Israel, 1996., Nineteenth Convention of*, pages 216–219.